CHIN. PHYS. LETT. Vol. 28, No. 6 (2011) 064301

A Baseline-Free Defect Imaging Technique in Plates Using Time Reversal of Lamb Waves *

Hyunjo Jeong**, Sungjong Cho, Wei Wei

Division of Mechanical and Automotive Engineering, Wonkwang University, Iksan, Jeonbuk 570-749, Korea

(Received 6 January 2011)

We present an analytical investigation for a baseline-free imaging of a defect in plate-like structures using the time-reversal of Lamb waves. We first consider the flexural wave (A_0 mode) propagation in a plate containing a defect, and reception and time reversal process of the output signal at the receiver. The received output signal is then composed of two parts: a directly propagated wave and a scattered wave from the defect. The time reversal of these waves recovers the original input signal, and produces two additional sidebands that contain the time-of-flight information on the defect location. One of the side-band signals is then extracted as a pure defect signal. A defect localization image is then constructed from a beamforming technique based on the time-frequency analysis of the side band signal for each transducer pair in a network of sensors. The simulation results show that the proposed scheme enables the accurate, baseline-free imaging of a defect.

PACS: 43.35.Cg, 43.60.Tj, 43.60.Lq DOI:10.1088/0256-307X/28/6/064301

Most of the Lamb wave-based damage detection techniques often require a past baseline data. The scattered signal from a damage is obtained using the baseline subtraction to construct the damage localization image.[1,2] A time reversal (TR) process can be established as a baseline-free method for damage detection in SHM applications.[3] Initial applications for the time reversal method in flaw or damage detection were aimed at increasing Lamb wave resolution by using time reversal mirrors.[4] The effect of dispersion on the time reversal analysis of Lamb waves was first studied by Wang *et al.*[5] by introducing the time reversal operator into the Lamb wave equation based on the Mindlin plate theory. Park *et al.*[6] demonstrated that the use of a narrowband toneburst excitation fully restores the original input signal through a single mode Lamb wave time reversal process. Xu and Giurgiutiu[7] and more recently Park *et al.*[8] proposed a theoretical model for studying the Lamb wave time reversal behavior in single and multiple modes, and verified it experimentally. In this Letter, we present an analytical investigation for defect localization image (detection and location) in plate-like structures using the time reversal analysis of flexural waves.

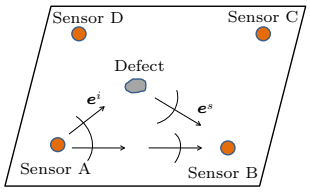

Fig. 1. Lamb wavebased defect localization using a network of sensors.

Figure 1 shows the testing components for damage/defect detection and localization where a flaw is being interrogated in a pitch-catch arrangement using a network of piezoelectric (PZT) transducers.

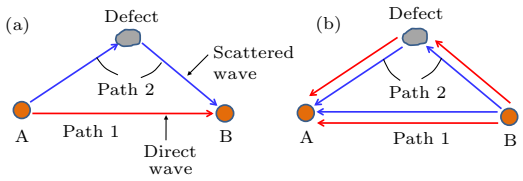

Fig. 2. Flexural wave propagation in a plate containing a defect: (a) forward propagation from sensor A, and (b) backward propagation from sensor B after reception and time reversal.

When the flexural Lamb wave is generated at sensor A and travels along the plate containing a defect, the forward propagating wave will arrive at sensor B through two different paths, as shown in Fig. 2(a). In Fig. 2, P_1 and P_2 represent the direct and scattering paths. The response voltage obtained at sensor B through the direct path P_1 can be written in the frequency domain as

$$V_{B1}(\omega) = G_1 K_a K_S V_{\rm A}, \tag{1}$$

where $V_{\rm A}$ is the input at patch A, K_a and K_s, the mechanical-electro efficiency factor of sensor A and B, and G_1 the frequency response function of sensor B as a result of the input at sensor A.[6]

On the other hand, the response signal at sensor B through the scattering path P_2 can be described by

$$V_{B2}(\omega) = G_{1S} G_{S2} A^{\boldsymbol{e}^i;\boldsymbol{e}^s} K_a K_S V_{\rm A} = G_2 K_a K_S V_{\rm A}, \tag{2}$$

where $G_2 = G_{1S} G_{S2} A^{\boldsymbol{e}^i;\boldsymbol{e}^s}$; G_{1S} and G_{S2} are the transfer functions for wave propagation paths from

*Supported by Basic Science Research Program (2010-0013901) and by the Nuclear R&D program through the National Research Foundation of Korea (NRF) funded by the Ministry of Education, Science and Technology.

**Email: ndejeong@hotmail.com; henryjoe@naver.com

© 2011 Chinese Physical Society and IOP Publishing Ltd

actuator 1 to the scatterer and from the scatterer to sensor 2, respectively; and $A^{e^i;e^s}$ is the far field scattering amplitude which completely describes the scattered wave field.[9]

Once a response signal is measured at sensor B, the reconstructed input signal at sensor A can be obtained by re-emitting the time-reversed response signal at sensor B. The time reversal operation of a signal in the time domain is equivalent to taking the complex conjugate of the Fourier transform of the signal in the frequency domain. There are four possible propagation paths when the received signal at sensor B is time reversed and re-emitted to reach sensor A. Therefore, the reconstructed signal at sensor A from the re-emitted signal at sensor B can be written as

$$V_R(\omega) = V_R^{11} + V_R^{22} + V_R^{12} + V_R^{21}, \tag{3}$$

where

$$\begin{aligned} V_R^{mn} &= G_m G_n^* K_a K_S K_a^* K_S^* V_{\rm A}^* \\ &= G_m G_n^* K K^* V_{\rm A}^*, \quad m,n = 1,2, \end{aligned} \tag{4}$$

Here superscript $*$ denotes the complex conjugate. In this formulation, the reciprocity of flaw scattering in forward and backward propagation is assumed for simplicity of analysis. Equation (3) now can be expressed as

$$V_R(\omega) = \sum_{m=1}^{2}\sum_{n=1}^{2} G_m G_n^* K K^* V_{\rm A}^*, \tag{5}$$

The properties of this reconstructed wave packet, Eq. (5), can be further explored if we look at its time domain signal via the inverse Fourier transform. For this purpose we introduce the transfer function for a point source. Then the transfer function for a flexural mode Lamb wave can be defined in the form of a plane wave solution,

$$G_m = a_m \exp(ikr_m), \tag{6}$$

where r_m denotes the mth traveling path. Substituting Eq. (6) into Eq. (5) yields

$$V_R(\omega) = \sum_{m=1}^{2}\sum_{n=1}^{2} C_{mn} e^{i\theta_{mn}} K K^* V_{\rm A}^*, \tag{7}$$

where $C_{mn} = a_{mn} a_n^*$ and $\theta_{mn} = k(r_m - r_n)$.

Reconstructed the input signal in the time domain can be obtained by taking inverse Fourier transform of Eq. (7),

$$v_R(t) = \sum_{m=1}^{2}\sum_{n=1}^{2} \frac{1}{2\pi}\int_{-\infty}^{\infty} C_{mn} K K^* V_{\rm A}^* e^{i(\theta_{mn}-\omega t)} d\omega, \tag{8}$$

When the original input signal is a narrowband toneburst with a center frequency of $\bar{\omega}$, Eq. (8) can be reduced to

$$v_R(t) = \sum_{m=1}^{2}\sum_{n=1}^{2} \frac{1}{2\pi}\int_{-\infty}^{\infty} \bar{C}_{mn} \bar{K} V_{\rm A}^* e^{i(\theta_{mn}-\omega t)} d\omega \tag{9}$$

where $\bar{C}_{mn} = a_m(\bar{\omega}) a_n^*(\bar{\omega})$ and $\bar{K} = K(\bar{\omega}) K^*(\bar{\omega})$. Because $\theta_{mn} = 0$ for $m = n$, Eq. (9) can be written as

$$\begin{aligned} v_R(t) = {} & V_{\rm A}(T-t) \sum_{m=1}^{2} \bar{C}_{mn} \bar{K} \\ & + \sum_{m=1}^{2}\sum_{n=1}^{2} (1-\delta_{mn}) \frac{1}{2\pi}\int_{-\infty}^{\infty} \bar{C}_{mn} \bar{K} V_{\rm A}^* \\ & \times e^{i(\theta_{mn}-\omega t)} d\omega, \end{aligned} \tag{10}$$

where δ_{mn} denotes the Kronecker delta. We obtain an approximate solution for the second term on the right hand side of Eq. (10) using the Taylor series expansion of θ_{mn} near the central frequency $\bar{\omega}$ up to the first order:

$$\theta_{mn} \approx \theta_{mn}(\bar{\omega}) + \left.\frac{d\theta_{mn}}{d\omega}\right|_{\omega=\bar{\omega}} (\omega - \bar{\omega}), \tag{11}$$

By using the relationship among the wave number k, the phase velocity v_p, and the group velocity v_g, $kv_p\omega$ and $d\omega/dk = v_g$, Eq. (11) can be rewritten as

$$\theta_{mn} = \bar{\omega}\bar{\tau}_{mn} + \omega \bar{t}_{mn}, \tag{12}$$

where

$$\bar{\tau}_{mn} = (r_m - r_n)\left[\frac{1}{\bar{v}_p} - \frac{1}{\bar{v}_g}\right], \quad \bar{t}_{mn} = \frac{r_m - r_n}{\bar{v}_g}, \tag{13}$$

In Eq. (12), $\bar{v}_p$ and $\bar{v}_g$ are the phase and group velocity at $\bar{\omega}$. With use of Eqs. (12) and (13), Eq. (10) can be finally written as

$$\begin{aligned} v_R(t) = {} & \sum_{m=1}^{2} \bar{C}_{mn} \bar{K} V_{\rm A}(T-t) + \sum_{m=1}^{2}\sum_{n=1}^{2} (1-\delta_{mn}) \\ & \times \bar{C}_{mn} \bar{K} e^{i\bar{\omega}\bar{\tau}_{mn}} V_{\rm A}[T - (t - \bar{t}_{mn})], \end{aligned} \tag{14}$$

Equation (14) shows that the reconstructed signal is composed of four terms. The first two terms on the right-hand side are produced when the time reversed direct and scattered waves travel back to sensor A (the original source position) along their respective forward propagation paths. They merge constructively at the same time to form a main part of the reconstructed voltage and thus represent the scaled and time-reversed version of the original input signal. It is noted that the reconstructed main signal have arrival time difference of $\bar{t}_{mn}$ compared to the second group of the reconstructed signal.

In addition to the reconstructed main signal, two other terms appear in Eq. (14). They represent the reconstructed signals when the direct and scattered waves travel along two different paths in the forward and backward propagation directions (i.e., $P_1 \to P_2$, $P_2 \to P_1$). The third term indicates the reconstructed voltage when the time reversed direct wave takes the path P_2 in its back propagation to sensor A. Compared

to the arrival time of the main signal, this wave will arrive later in time. The fourth term indicates the reconstructed voltage when the time reversed scattered wave takes the path P_1 in its back propagation to sensor A. This wave will appear before the main signal. In other words, they are time shifted by $\bar{t}_{mn}$ and since $\bar{t}_{mn} = -\bar{t}_{nm}$ they create side bands with respect to the reconstructed main signal.

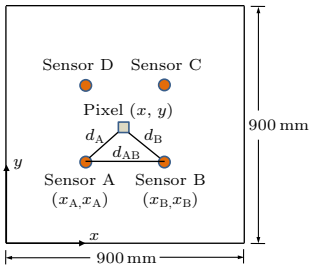

Fig. 3. A beamforming method to construct a defect localization image based on a network of four sensors. Sensor coordinates: A (300, 300), B (600, 300), C (600, 600), D (300, 600) in units of mm.

A beamforming method can be used to construct a defect localization image (location and imaging) by relating the contrast at a particular pixel to the amplitude of the scattered signal received by all the sensors in the network. Consider a distributed network consisting of N active sensors, their positions being denoted by (x_i, y_i), $i = 1, 2, \cdots, N$. The contrast S at a particular location or imaging pixel (x, y) can be expressed as

$$S(x,y) = \sum_{A=1}^{N} \sum_{B=1, B\neq A}^{N} W_{AB} f_{AB}(t_{AB}(x,y)), \qquad (15)$$

where W_{AB} refers to the appropriate aperture weighting to each sensor pair and $f_{ij}(t)$ denotes the received scattered signal by sensor j due to the excitation of sensor i. Referring to Fig. 3, the arrival time t_{AB} of the scattered wave corresponds to the wave travel time from the actuator to the defect and then from the defect to the sensor is

$$t_{AB}(x,y) = \frac{[d_A(x,y) + d_B(x,y)] - d_{AB}}{v_g}, \qquad (16)$$

with

$$d_A(x,y) = \sqrt{(x_A - x)^2 + (y_A - y)^2},$$
$$d_B(x,y) = \sqrt{(x_B - x)^2 + (y_B - y)^2},$$

where d_A and d_B are the distances from the transducer A (actuator) to the defect and from the defect to the transducer B (sensor), respectively; d_{AB} is the direct distance from A to B; v_g is the group velocity of the flexural Lamb wave. In the present case, three through-transmission signals can be obtained when one particular transducer is excited. Therefore there are a total of twelve different signals corresponding to the twelve possible sensor pair combinations.

In the following numerical simulation, the frequency $f = 150\,\text{kHz}$ and the number of cycles $N = 5$ are used (Fig. 4(a)). An aluminum plate ($E = 73\,\text{GPa}$, $\nu = 0.33$, $\rho = 2700\,\text{kg/m}^3$, $h = 1.0\,\text{mm}$) is used. A 2-mm-diameter circular hole is located at $(x_d, y_d) = (450\,\text{mm}, 450\,\text{mm})$.

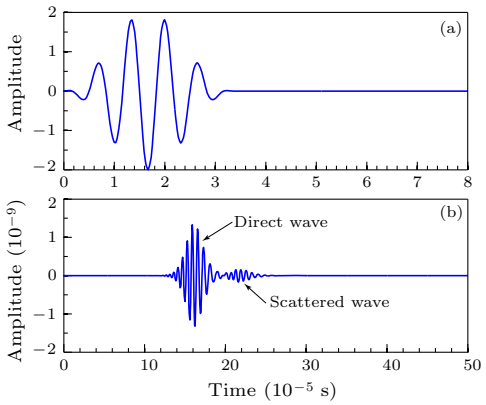

Fig. 4. (a) Time domain input signal of 150 kHz central frequency, and (b) response signal at sensor B for simulation configuration in Fig. 2(a).

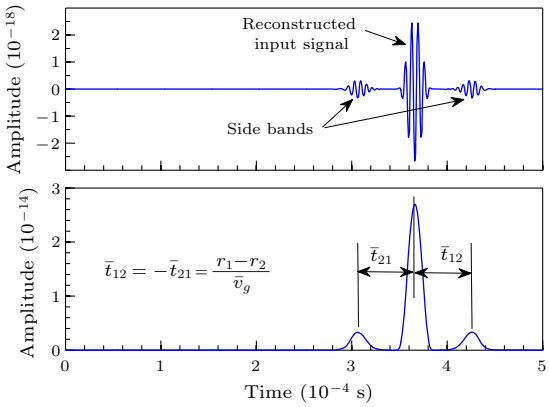

Fig. 5. Reconstructed signal at sensor A after time reversal and re-emission of received signal at sensor B together with the arrival time difference between the main mode signal and the side bands.

The response signal received at sensor B is shown in Figs. 4(b). The received signal is composed of the direct wave and the scattered wave. The scattering amplitude in Eq. (2) was calculated from the closed form solution for circular holes.[9] Two side bands appear with respect to the main signal. It is noted from Eq. (11) that $\bar{t}_{12}$ and $\bar{t}_{21}$ are the same time shift with the opposite signs $\bar{t}_{12} = -\bar{t}_{21}$, and this is clearly reflected on a symmetric pair of the side bands in Fig. 5. The time difference $\bar{t}_{mn}$ between the main mode and one of the side bands is calculated by

$$(r_2 - r_1)/\bar{v}_g = (d_A + d_B - d_{AB})/\bar{v}_g$$
$$= (0.3\sqrt{2} - 0.3)/2069 = 60\,\mu\text{s}.$$

From Fig. 5, this time difference is also estimated to be 60 μs from the wavelet transform signal processing

of received signal.[10] The reconstructed input signal is magnified in the vicinity of the main mode and compared to the original input signal in Fig. 6. The shape of the reconstructed main mode is practically identical to that of the original input signal.

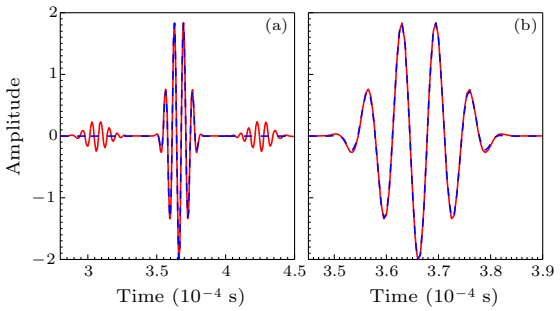

Fig. 6. Reconstructed main mode signal completely recovers the original input signal: (a) comparison of the whole signal and (b) magnification of the main mode signal.

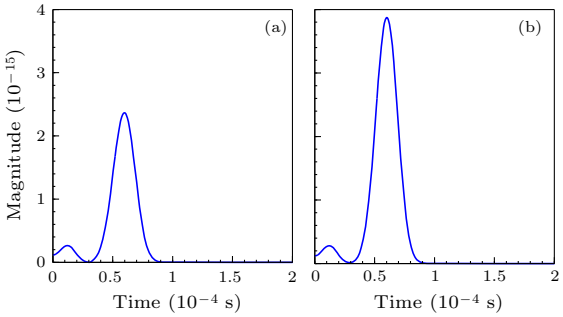

Fig. 7. Extracted defect signal envelopes: (a) for a sensor pair of A and B, (b) for a sensor pair of A and C.

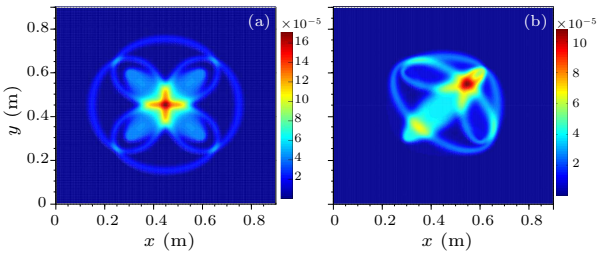

Fig. 8. Defect localization images of a 1-mm-radius hole: (a) defect location (450 mm, 450 mm) and (b) defect location (550 mm, 550 mm).

Figure 7 shows the time-frequency spectrum of the extracted defect signal (one of the side bands) after time reversal of the output signal and subtraction of the original input signal for sensor pair A–B and A–C, respectively. They correspond to defect scattering for 90° and 0° in Fig. 3, respectively, and well reflect the scattering amplitude difference at these angles. These spectra will be used for reconstructing the defect localization image.

The reconstructed defect localization image is shown in Fig. 8(a), where the circular through hole of 1 mm radius is located at the center of the sensor network, $(x_d, y_d) = (450\,\text{mm}, 450\,\text{mm})$. It shows that the reconstructed defect localization image accurately locates at the defect. This defect reconstruction is obtained by superimposing the images of different actuator/sensor signal paths. The next case aims to study the performance of Lamb wave-based defect detection methodology under a situation where the defect is located relatively close to one of the transducers in order to verify the robustness of the proposed methodology. Figure 8(b) shows the reconstructed defect localization image when the circular hole of 1 mm radius is located at $(x_d, y_d) = (550\,\text{mm}, 550\,\text{mm})$. The resulting image also accurately locates at the defect position.

In summary, a baseline-free imaging for detection and location of a defect in plates has been studied. The proposed method employs the time reversal of flexural waves and a beamforming technique using a distributed network of transducers operating in a pitch-catch mode. The time reversal of the output signal which contains the direct and scattered waves recovers the original input signal and produces additional side bands. One of the side band is used to form the baseline-free defect localization image. The simulated results of defect localization image show that the proposed technique accurately located the defect position.

References

[1] Ng C T and Veidt M 2009 *Smart Mater. Struct.* **18** 074006
[2] Zhang H Y, Chen X H, Cao Y P and Yu J B 2010 *Chin. Phys. Lett.* **27** 104301
[3] Sohn H, Park H W, Law K H and Farrar C R 2007 *J. Aerospace Eng.* **20** 141
[4] Fink M 1992 *IEEE Trans. UFFC* **39** 555
[5] Wang C H, Rose J T and Chang F K 2004 *Smart Mater Struct.* **13** 415
[6] Park H W, Sohn H, Law K H and Farrar C R 2007 *J. Sound Vib.* **302** 50
[7] Xu B and Giurgiutiu V 2007 *J. Nondestr. Eval.* **26** 123
[8] Park H W, Kim S B and Sohn H 2009 *Wave Motion* **46** 451
[9] Norris A N and Vemula C 1995 *J. Sound Vib.* **181** 115
[10] Jeong H and Jang Y-S 2000 *IEEE Trans. UFFC* **47** 612